Recommendations for Velocity Adjustment in Surface Hopping

Josene M Toldo, Rafael S Mattos, Max Pinheiro, Saikat Mukherjee, Mario Barbatti

Recommendations for velocity adjustment in surface hopping

Josene M. Toldo[1*], Rafael S. Mattos,[1] Max Pinheiro[1], Saikat Mukherjee[1], Mario Barbatti[1,2*]

[1] *Aix-Marseille University, CNRS, ICR, Marseille, France,*
[2] *Institut Universitaire de France, 75231, Paris, France*

Abstract. This study investigates velocity adjustment directions after hoppings in surface hopping dynamics. Using fulvene and a protonated Schiff base (PSB4) as case studies, we investigate the population decay and reaction yields of different sets of dynamics with the velocity adjusted either in the nonadiabatic coupling, gradient difference, or momentum directions. For the latter, besides the conventional algorithm, we investigated the performance of a reduced kinetic energy reservoir approach recently proposed. Our evaluation also considered velocity adjustment in the directions of approximate nonadiabatic coupling vectors. While results for fulvene are susceptible to the adjustment approach, PSB4 is not. We correlated this dependence to the topography near the conical intersections. When nonadiabatic coupling vectors are unavailable, the gradient difference direction is the best adjustment option. If the gradient difference is also unavailable, a semiempirical vector direction or the momentum direction with a reduced kinetic energy reservoir becomes an excellent option to prevent an artificial excess of back hoppings. The precise velocity adjustment direction is less crucial for describing the nonadiabatic dynamics than the kinetic energy reservoir's size.

VOR: J. Chem. Theory Comp, doi: 10.1021/acs.jctc.3c01159

1 Introduction

Modelling the dynamics of photochemical and photophysical processes requires coupling nuclear and electronic degrees of freedom beyond the adiabatic regime.[1, 2] Surface hopping is a mixed quantum-classical method that conveniently allows simulating these processes. It computes molecular dynamics involving multiple electronic states—that is, nonadiabatic dynamics—by evolving a swarm of independent trajectories, where the nuclei are propagated classically, and the electronic part is computed quantically at each time step.[3] Each trajectory is propagated on a single electronic state but can hop and continue on another, as determined by the specific surface hopping algorithm. The swarm of independent trajectories evolving through multiple states is an approximation for the quantum nuclear wave packet.[4]

The decision regarding whether the molecules should continue in the same state or hop to another state is controlled by a stochastic process. The hopping event between states tends to occur at small but finite potential energy gaps, where nonadiabatic couplings are significant. Although the energy gap distribution is system-dependent, an exponential distribution with a mean value of about 0.2 to 0.5 eV is often observed.[5] There are also reports of Gaussian distributions of energy gaps with similar mean values,[6] and even convolutions of exponential and Gaussian distributions with different mean values.[7]

The energy gap at the hopping time implies that if the trajectory hops from a higher to a lower state, its potential energy instantaneously drops. On the other hand, its potential energy rises if it hops from a lower to a higher state (back hopping). Therefore, after a successful hop, we must adjust the nuclear kinetic energy to compensate for the potential energy variation to conserve the total energy.

It may also happen that when attempting to hop to a higher state, no kinetic energy reduction can enforce energy conservation. In this case, the standard procedure is to keep the trajectory on the same surface (frustrated hopping). Other options are also available to ensure energy conservation, for example, by incorporating quantum uncertain into the hopping times of classically forbidden hops.[8] Recently, modifications in the formulation of the derivative coupling to allow the conservation of linear and angular momentum have been proposed to find a meaningful momentum rescaling direction after hops.[9]

Herman claimed in a series of works that only the momentum component parallel to the nonadiabatic coupling vector should change in adiabatic[10, 11] or any other representation.[12] His conclusion stems from a semiclassical treatment of nonadiabatic dynamics for multidimensional scattering problems. He showed that one-dimensional transition amplitudes satisfy the semiclassical Schrodinger equation if all order terms are evaluated by altering the momentum in the direction of the nonadiabatic coupling vector to conserve total energy after the transition.[11]

Tully followed a different path to show that the momentum should be corrected in the nonadiabatic coupling vector direction.[3] He computed the Pechukas force,[13] which is the semiclassical force driving the most critical classical-like path in a two-state quantum system. This force has three components at any time: two along the potential energy gradients of the current and target electronic states and the third along the nonadiabatic coupling vector between them. This third component (Tully calls it a *transition force*) is the only one proportional to the potential energy gap, which leads to conclude that it enforces the energy conservation during the nonadiabatic transition.

Despite being consensual that the nuclear momentum (or equivalently, the nuclear velocity) should be corrected in the coupling vector direction, it is not always possible to do so because the direction information may not be available. Certain varieties of surface hopping skip the coupling vector calculation.[14] Such is the case of the fewest switches based on local diabatization,[15, 16] time-derivative couplings,[17, 18] Belyaev-Lebedev couplings,[7, 19, 20] time-dependent Baeck-An couplings,[21] and Zhu−Nakamura surface hopping.[22] In most of those cases, the common practice is enforcing energy conservation by changing the nuclear velocity in the direction of the momentum. In Zhu-Nakamura surface hopping, velocities are changed in the direction of the diabatic-energy gradient-difference vector at the minimum energy gap. Another situation where velocity adjustment cannot be done in the direction of the nonadiabatic coupling vector is when surface hopping is based on the neglect of back-reaction approximation.[23] In this case, the hoppings between states are evaluated on a pre-computed ground-state trajectory; therefore, the velocity cannot be altered. An artificial excess of back hoppings

is avoided by weighting the hopping probability by a statistical factor reflecting the system's probability of accumulating kinetic energy amount above the energy gap.[24]

Recently, we realized that the surface hopping results for highly excited pyrene were qualitatively wrong when velocity was adjusted along the momentum.[25] To deal with this issue, we proposed an adjustment of the velocity, which divides the total kinetic energy before hopping by the number of vibrational degrees of freedom when still using velocity adjustment in the momentum direction. This adjustment significantly reduces the number of back hoppings for pyrene.

This paper investigates the performance of this and other velocity adjustment models. We benchmark them for two systems, fulvene and the protonated Schiff base *cis*-PSB4 (5-*cis*-hepta-3,5,7-trieniminium cation), shown in **Figure 1**. We start by reviewing velocity adjustment in surface hopping. Then, we investigate the dynamic propagation and the significance of the statistical errors when velocity is adjusted in different directions compared to the direction of the nonadiabatic coupling vector. We link our findings to the topography of the conical intersections in fulvene and PSB4. Finally, we extended our discussion to encompass the curvature-driven approximation for the nonadiabatic coupling vector[26] and tested a hybrid algorithm that computes the nonadiabatic coupling vectors during surface hopping using an inexpensive semiempirical method.

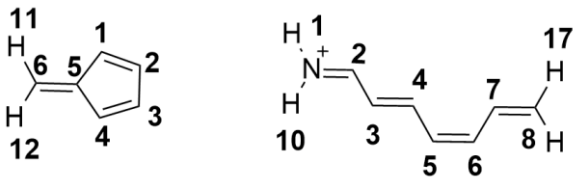

Figure 1. Molecular structures and numbering of fulvene and 5-*cis* isomer of PSB4.

2 Velocity Rescaling in Surface Hopping

Ibele and Curchod reported significant differences in the nonadiabatic dynamics of fulvene in decoherence-corrected surface hopping when the velocity is adjusted in the momentum or nonadiabatic coupling vector directions.[27] Barbatti showed for surface hopping of ethylene that the error caused by not changing the velocity in the nonadiabatic coupling direction tends to be hidden by the statistical error of small trajectory ensembles.[28] Limbu and Shakib used different schemes of velocity rescaling to treat frustrated hops in the context of ring polymer surface hopping.[29] They evaluated whether the velocity should be reversed in the case of frustrated hops and their effects on preserving the correct quantum dynamics. They found that reversing the velocity after frustrated hops induces quantum back reactions, improving detailed balance in low to high temperatures. Still, they recommend caution when choosing the treatment because it may fail in some systems.

Two problems are associated with not rescaling the nuclear velocity in the nonadiabatic coupling vector direction. First, the momentum added to another direction after hopping may induce wrong reaction pathways. Second, specific alternative directions, like linear momentum, are defined in the entire molecular system and not restricted to the nonadiabatically coupled region. This leads to size-

extensivity issues that we discuss later in this section and causes an excess of back hoppings, as mentioned in the Introduction.

The literature record is undecisive concerning the first problem. On the one hand, results by Fernandez-Alberti, Tretiak, and co-authors[30, 31] imply that the momentum direction after hopping is unimportant. These authors showed for different systems that, although dynamics evolve in the nonadiabatic coupling vector direction immediately before internal conversion, after internal conversion, the system's dynamics do not strongly correlate with the coupling vector direction. On the other hand, retinal models' isomerization quantum yield is sensitive to details of the momentum allocation after hopping due to hydrogen out-of-plane vibrational modes.[32] Ref. [33] also reports a strong correlation between the exit direction in the crossing seam and the photoproduct.

Regarding the second problem, suppose a hopping from a lower state L to an upper state J is attempted over a potential energy gap ΔE_{LJ}. As we showed before,[25] such back hopping is allowed if kinetic energy variation $\Delta K_{LJ} = -\Delta E_{LJ}$ satisfies

$$\left|\Delta K_{LJ}\right| \leq \frac{1}{2\sum_{\alpha}\frac{u_{\alpha}^{2}}{M_{\alpha}}}\left(\sum_{\alpha}\mathbf{v}_{\alpha}^{(L)}\cdot\mathbf{u}_{\alpha}\right)^{2} \tag{1}$$

where α runs over all atoms. For each atom, M_α is the mass, $\mathbf{u}_\alpha$ is the vector indicating the velocity adjustment direction and $\mathbf{v}_{\alpha}^{(L)}$ is the velocity before hopping. This inequality is derived in the Supporting Information section SI-1 and Ref [25].

The right side of this inequality is the kinetic energy reservoir, $T(\mathbf{u})$, which ensures energy conservation. It is controlled by the orientation between $\mathbf{v}^{(L)}$ and $\mathbf{u}$. If the adjustment is made in the nonadiabatic coupling vector direction $\mathbf{h}_{LJ}$, the kinetic energy reservoir is

$$T\left(\mathbf{h}_{LJ}\right) = \frac{1}{2\sum_{\alpha}\frac{\left(h_{LJ,\alpha}\right)^{2}}{M_{\alpha}}}\left(\sum_{\alpha}\mathbf{v}_{\alpha}^{(L)}\cdot\mathbf{h}_{LJ,\alpha}\right)^{2} \tag{2}$$

which depends on the projection of $\mathbf{v}^{(L)}$ on $\mathbf{h}_{LJ}$. In this equation, the nonadiabatic coupling vector is defined for each nucleus α as

$$\mathbf{h}_{JI,\alpha}(\mathbf{R}) \equiv \left\langle \Psi_J(\mathbf{R}) \middle| \nabla_{\alpha} \Psi_I(\mathbf{R}) \right\rangle \tag{3}$$

where $\Psi_J(\mathbf{R})$ is the electronic wave function of state J (and equivalent for I) at nuclear geometry $\mathbf{R}$, and the gradient is taken in the nuclear coordinate $\mathbf{R}_\alpha$.

On the other hand, when the adjustment is made in the direction of the momentum before hopping $\mathbf{p}^{(L)}$, the kinetic energy reservoir is simply

$$T\left(\mathbf{p}^{(L)}\right) = \frac{1}{2}\sum_{\alpha} M_{\alpha}\left(\mathbf{v}_{\alpha}^{(L)}\right)^{2} = K_L \tag{4}$$

the total kinetic energy K_L before hopping.

Thus, only a subset of atoms contributes to the kinetic energy reservoir $T(\mathbf{h}_{LJ})$ (those in the molecular region causing the state crossing), while all atoms contribute to $T(\mathbf{p}^{(L)})$. The direct implication of having a bigger reservoir for the latter is that adjusting the velocity along $\mathbf{p}^{(L)}$ should enable many more back hoppings than when changing along $\mathbf{h}_{LJ}$.

This size-extensivity problem has been recognized before, as the Introduction surveys. Plasser *et al.*[34] reported a benchmark study of a 15D model Hamiltonian with a high density of states, comparing surface hopping and wave packet propagation. They noticed significant differences between results with adjustment along momentum and coupling vector. They also reported that adjustment in the gradient difference vector $\mathbf{g}_{LJ}$ worked well, which was rationalized statistically. What matters the most is not the precise direction but adjusting the velocity along a single degree of freedom (done with both **g** and **h**, but not **p**).

Some of us have recently shown that surface hopping results for highly-excited pyrene (72D) were qualitatively wrong when velocity was adjusted along the momentum.[25] Following the insight of Ref. [34] that reducing the dimensionality of the adjustment direction is vital, we defined an *ad hoc* reduced kinetic energy reservoir

$$T_{RED}\left(\mathbf{p}^{(L)}\right) = \frac{K_L}{N_{DF}} \tag{5}$$

which divides the total kinetic energy before hopping by the number of vibrational degrees of freedom N_{DF}. In practical terms, the velocity adjustment is still made in the momentum direction, but back hoppings are accepted only if the energy gap satisfies the inequality

$$\frac{K_L}{N_{DF}} - \Delta E_{LJ} \geq 0 \tag{6}$$

Therefore, this size-extensivity correction prevents an artificial excess of back hoppings when the velocity is adjusted along the momentum. The justification for this *ad hoc* approximation considers that the nonadiabatic coupling vector is the recommended direction for velocity adjustment, and this vector corresponds only to one degree of freedom. Therefore, dividing the whole kinetic energy available by the total number of degrees of freedom should deliver a sensible approximation. This simple modification worked perfectly for pyrene,[25] which led us to explore it in further detail for different systems, as we report below.

3 Computational Methods

3.1 Fulvene

We chose two model systems to investigate the velocity adjustment direction and dimentionality reduction[25] during surface hopping dynamics. The first one is fulvene (**Figure 1**). We applied the

complete active space self-consistent field (CASSCF) method to run seven sets of surface hopping dynamics for this molecule. Using nonadiabatic coupling vectors to evaluate the hopping probability, we computed dynamics adjusting the velocity in the (i) nonadiabatic coupling vector direction (**h**-adjusted set), (ii) the gradient difference vector direction (**g**-adjusted set), (iii) the momentum direction (**p**-*fullKE*-adjusted set) with full kinetic energy reservoir, (iv) the momentum direction with reduced kinetic energy reservoir (**p**-*redKE*-adjusted set), and (v) a semiempirical nonadiabatic coupling vector direction.

The **p**-*fullKE*-adjusted set (set iii) refers to the velocity adjustment in the original momentum direction using all kinetic energy available according to eq. (4). In contrast, the **p**-*redKE*-adjusted set (set iv) uses the eq. (5) to adjust the velocity. The goal of set v is to test the adjustment using **h** vectors obtained with an inexpensive semiempirical technique, which could be invoked even when the electronic structure method adopted for dynamics propagation does not allow computing them. Two additional data sets using the time-derivative Baeck-An (TD-BA)[21] model were computed using **p**-adjustment using (vi) full kinetic energy and (vii) reduced kinetic energy.

The reduced kinetic energy approach is only used to determine if a back hopping will occur without impacting other surface hopping propagation features. In the case of frustrated hops, the momentum direction was kept. For up-to-down hops, we adjust the velocity as usual, considering the full kinetic energy.

In all cases, an active space composed of 6 electrons in 6 orbitals state-averaged over two states [SA-2-CAS(6,6)] was used. This active space contains the 3 π and 3 π* molecular orbitals of fulvene. The 6-31G(d)[35] basis set was employed. Conical intersections were also optimized at this level of theory. The MCSCF calculations were done with Columbus (version 7.0.1_2021-01-14).[36, 37]

Dynamics simulations were performed using the fewest-switches surface hopping approach (FSSH)[38] with decoherence-corrections (0.1 au)[39] as implemented in Newton-X CS (version 2.5 build 05)[40] interfaced with Columbus. The initial conditions for the dynamics were sampled from a harmonic oscillator Wigner distribution of the nuclei. They were restricted to a 4.00 ± 0.34 eV window and began from the S_1 state. We ran 200 trajectories up to 60 fs for each dataset using the velocity-Verlet[41] algorithm with a timestep of 0.1 fs. The quantum equations were integrated using interpolated electronic quantities between classical steps with a time step of 0.005 fs. Except for TD-BA dynamics, which uses time-dependent Baeck-An couplings, exact nonadiabatic coupling vectors were computed for all the data sets. The TD-BA model was applied using analytical second derivatives from quadratic regression (ΔT = 0.4 fs) and $\delta\eta$ = 0.1 au.

We also tested a hybrid method, which uses the CASSCF nonadiabatic coupling vectors to evaluate FSSH probabilities but rescales the velocity in the direction of semiempirical nonadiabatic coupling vectors computed with the floating occupation molecular orbital configuration interactions (FOMO-CI) method.[42] In this case, the active space also contains six electrons in six orbitals. FOMO-CI was done with a development version of MOPAC.[43, 44]

3.2 PSB4

Our second model system is the *cis*-hepta-3,5,7-trieniminium cation (PSB4, **Figure 1**). For this molecule, we performed four sets of surface hopping dynamics using different velocity adjustment directions: the nonadiabatic coupling vector (**h**), the gradient difference (**g**), and the momentum (**p**) using full and reduced kinetic energy reservoirs. In the case of a frustrated hopping, the momentum direction was not modified.

The calculations were performed using CASSCF following the procedure and classification scheme described in Szymczak *et al.*[45] Here, however, we did not use mechanical restrictions to emulate the protein environment. The active space was composed of eight electrons distributed in eight orbitals (four π and the corresponding four π* orbitals) and averaged over two states [SA-2-CASSCF(8,8)]. Conical intersections were also optimized at this level of theory using Columbus software. All the calculations were performed using the 6-31G(d) basis set.

The initial conditions for the dynamics were sampled from a quantum harmonic oscillator Wigner distribution around the ground-state equilibrium geometry calculated at SA-2-CASSCF(8,8) level. 300 geometries and velocities were generated within an excitation window of 3.91 ± 0.6 eV. For each of the four datasets, 100 FSSH trajectories were computed starting from the S_1 state. They were propagated for up to 300 fs. A classical time step of 0.2 fs was used within the velocity-Verlet algorithm. The time-dependent Schrodinger equation was integrated with 0.005 fs steps. Time-dependent adiabatic populations were corrected for decoherence effects[46] (0.1 a.u.). The simulations were conducted using Newton-X CS interfaced with Columbus.

3.3 Data Analysis

Classification of hopping geometries of fulvene. The classification scheme for the hopping geometries in fulvene is based on our previous publication.[21] The ultrafast dynamics of fulvene is characterized by an extended crossing seam with the torsion involving the exocyclic double bond varying from planar to 90° twisted structures.[47-49] To evaluate these structural changes, we considered a mean torsional angle (ϕ_{C-CH_2}) composed of the average of the absolute values of the four dihedral angles around the exocyclic double bond

$$\phi_{\text{C-CH}_2} = \frac{1}{4}\left[\left|\phi^{cis_1}_{\text{CC-CH}}\right| + \left|\phi^{cis_2}_{\text{CC-CH}}\right| + \left|180^\circ - \phi^{trans_1}_{\text{CC-CH}}\right| + \left|180^\circ - \phi^{trans_2}_{\text{CC-CH}}\right|\right] \quad (7)$$

Three regions in the crossing seam were defined to compare the datasets. The first region includes near-planar structures ($\phi_{C-CH_2} \geq 30°$); the second region comprises twisted-stretched structures ($\phi_{C-CH_2} \geq 30°$ and $C–CH_2 > 1.55$ Å); and the third region includes twisted-shrunk geometries ($\phi_{C-CH_2} \geq 30°$ and $C–CH_2 < 1.55$ Å).

The margin of error for the proportion p_i of each type of hopping geometry was computed (with $Z = 1.96$ for a 95% confidence interval) as

$$\varepsilon = Z\sqrt{\frac{p_i(1-p_i)}{N_{traj}}} \tag{8}$$

Classification of hopping geometries for PSB4. The classification scheme for the hopping geometries of PSB4 was based on Szymczak *et al.*[45] In PSB4, several photoisomerization pathways can occur. The motions leading to the conical intersections were categorized in terms of the relative changes of the dihedral angles ($\Delta\theta_i$) at the hopping moment. These dihedrals are defined considering the heavy atoms along the PSB4 chain; for terminal torsions, a *trans* hydrogen atom was used. **Table S1** shows the patterns for the different hopping geometries according to their dihedral angle changes. The values for $\Delta\theta_i$ are classified into three ranges: a ($0 \le \Delta\theta_i \le 30^\circ$), b ($30 < \Delta\theta_i \le 60^\circ$), and c ($60 < \Delta\theta_i \le 90^\circ$). The margin of error for the sample proportion of each type of hopping geometry was computed as mentioned for fulvene above.

The lifetime of PSB4 was fitted with the exponential decay function

$$f(t) = \exp(-(t - t_d)/t_e) \tag{9}$$

and the lifetime is given as $\tau = t_d + t_e$. The margin of error (with 95% confidence) was computed as

$$\delta_\tau = \frac{Z}{\sqrt{N_{traj}}} t_e \tag{10}$$

Statistical analysis. Comparing the sets of trajectories for both molecules followed the procedure presented in Ref.[50] This procedure allows us to check quantitatively how good the agreement between two datasets is by estimating the probability that they produce overlapping results with a given confidence interval (we used 95%). For fulvene, mean values and margin of errors were computed for six observables (first decay time constant, S_1 population at 20 fs, S_1 population at 60 fs, and three kinds of hopping geometries), as previously defined in Ref.[21] For PSB4, we evaluated five observables (excited state lifetime and four kinds of hopping geometries). An overlap score λ_x,[50] which measures the overlap between two datasets, was computed for each observable, taking the **h**-data set as a reference. This function varies between 0 (complete disagreement with reference data) and 1 (perfect agreement). The statistical analysis was done using ULaMDyn package (www.ulamdyn.com).

4 Results and Discussion

4.1 Nonadiabatic dynamics of fulvene

The nonadiabatic dynamics of fulvene has been extensively discussed in the literature. Due to its ultrafast excited state decay and small size, this molecule is an excellent model system for probing new implementations, and it has been proposed as a 3D molecular analog to the Tully model.[27] Among the different approaches used to investigate the excited state dynamics of fulvene, we can mention wavepacket propagation in reduced-dimensionality,[51-55] full-dimensionality direct-surface wavepacket propagation,[56, 57] multiple spawning,[27] and surface hopping.[21, 27, 47]

Upon photoexcitation to the S_1 state, fulvene can follow different decay pathways involving various conical intersections.[47, 53, 56, 57] An extended S_1/S_0 seam allows the population to return to the S_0 state through a range of geometries varying from planar to 90° twisted ones.[21, 47-49] The major part of the population decays via planar conical intersections, driven by a stretch of the $C{=}CH_2$ bond, involving a strongly sloped conical intersection, as also shown in our simulations (see **Figure S2** and **Table S3**). A smaller fraction of the population follows an alternative mechanism, returning to the S_0 state via a twist of the $C{=}CH_2$ bond. When the twist is complete and accompanied by a stretch of the same bond, the conical intersection is peaked, while when this torsion is partial, the slope is smoothed.

In **Figure 2**, we present the S_1 decay population of fulvene using different velocity adjustment directions. Except for the data sets using momentum direction and full kinetic energy reservoir, the other datasets show the same general behaviour. After excitation, fulvene returns to the S_1 state within the first 10 fs of simulation. A recurrent repopulation of the S_1 state at ~20 fs and ~40 fs can also be seen. It is indicated as broad peaks in those regions, particularly prominent in the two **p**-*fullKE* data sets. This fulvene S_1 population decay dependence on the velocity-adjustment direction has been recognized before.[27]

The peculiar peak in the 15 to 25 fs region stems from the strongly sloped conical intersection,[21, 27] characterized in the Supporting Information (**Section SI-3**). This topography causes part of the population that hops to S_0 almost immediately to return to the upper state. The prominent peaks in the two **p**-adjusted with full kinetic energy datasets are due to their large number of back hoppings (**Table 1**). When we keep the momentum direction but use the reduced kinetic energy, we get a much smaller number of back-hoppings, significantly improving the S_1 population decay. It is comparable to the velocity adjustment in the nonadiabatic coupling vector direction, unquestionably the most adequate direction.[28] The number of back hoppings is also significantly smaller for the **g**-adjusted set, for which the S_1 population decay also nicely agrees with the reference.

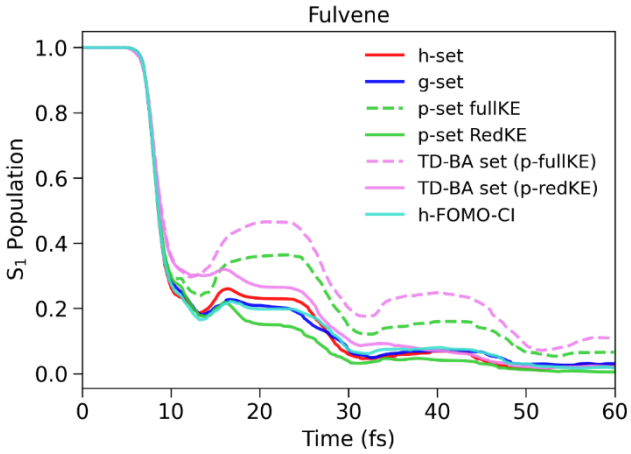

Figure 2. Excited state population of fulvene at the first 60 fs computed with different velocity adjustments after hoppings.

Given the striking difference in the dynamics observed for the **p**-adjusted *fullKE* datasets, we inquired ourselves what would happen if, after a hopping, we used an inexpensive method to compute nonadiabatic coupling vectors just to deliver the adjustment direction. If this hybrid scheme worked, it could be extended to approaches that do not count on coupling vectors, as those mentioned in the Introduction. This query motivated us to propose a modified scheme that uses the nonadiabatic coupling vectors computed with the semiempirical FOMO-CI only to adjust velocities after hoppings. Our results show that the population decay calculated by this hybrid method (**h**-FOMO-CI in **Figure 2**) closely matches the exact **h**-adjustment data set and perfectly agrees with the S_1 decay given by the **g**-dataset. We discuss this hybrid method in more detail in Section 4.3.2.

Table 1. Number of back hoppings for fulvene and PSB4 using different velocity adjustments after a hopping event: **h** set (along the nonadiabatic coupling vector); **g** set (along the gradient difference vector); **p** set (along the momentum direction) using conventional adjustment (*full KE*) and reduced kinetic energy (*Red KE*) adjustment.

	fulvene						**PSB4**			
	CASSCF				**TDBA**		**CASSCF**			
	h dataset	**g** dataset	**p** dataset		**p** dataset		**h** dataset	**g** dataset	**p** dataset	
			full KE	*Red KE*	*full KE*	*Red KE*			*full KE*	Red KE
# hoppings	227	223	261	209	268	199	103	100	109	103
# back hoppings	32	29	74	10	90	3	5	3	12	5
# frustrated hoppings	48	61	0	95	0	161	14	14	0	15
# trajectories with no hops	0	2	3	1	3	4	2	3	3	2

To provide a meaningful quantitative comparison between the datasets, we performed a statistical analysis following the protocol defined in our previous publications[21, 28] (see Section 3.3). **Table 2** shows the overlap score for the S_1 population at different times and structural changes of fulvene at the hopping times, as presented above. As expected, most of the population (~90%) decays via planar conical intersections, and only a tiny fraction decays via twisted intersections. For each of the three hopping regions (planar, twisted-stretched, and twisted-shrunk), the overlap scores are above 0.7, meaning that the datasets quantitatively agree. Exceptions are seen for TD-BA **p**-adjusted (as previously reported) and the twisted-shrunk geometries. Still, this last could result from the bad statistics reminiscent of the small number of trajectories falling in this region. When we turn to the lifetime and S_1 population, the agreement is overall much worse, as they have λ_x^h values closer to zero. Nevertheless, this divergence is not particularly critical in this case, as it indicates that TD-BA and **p**-adjusted *fullKE* decay are slightly slower than the reference dataset (**h**-set). Furthermore, the **g**-dataset

is in excellent agreement with the reference, and the **p**-reduced dataset shows a larger divergence only in the S_1 population at 20 fs.

Overall, these results indicated that if nonadiabatic couplings cannot be computed, the **g**-direction is the best choice, as it provides results in close agreement with the exact nonadiabatic coupling vector. If **g** is also unavailable (sometimes it is too costly to get energy gradients for all states), adjusting the velocity in the **p**-direction and using the reduced kinetic energy reservoir would give meaningful results for the excited state population evolution and reaction yields.

Table 2. Mean value and error bars (95% confidence interval) of time constants, populations, and structural yields computed for fulvene dynamics with different velocity adjustments after a hopping event. Results for **h**-adjusted, **g**-adjusted, and **p**-adjusted using full kinetic energy (*fullKE*) and reduced kinetic energy (*RedKE*). λ_x^h is the overlap score for each observable computed between **h**-adjusted (at CASSCF level) and the respective dataset.

	CASSCF							TD-BA			
Observable	**h** dataset	**g** dataset	λ_x^h	**p** *fullKE* dataset	λ_x^h	**p** *RedKE* dataset	λ_x^h	**p** *fullKE* dataset	λ_x^h	**p** *RedKE* dataset	λ_x^h
1st decay time τ_1 (fs)	11 ± 1	11 ± 1	1.00	12 ± 1	0.25	11 ± 1	1.00	14 ± 1	0.00	14 ± 1	0.00
S_1 population at 20 fs (%)	23 ± 6	21 ± 6	0.86	36 ± 7	0.00	15 ± 5	0.02	46 ± 7	0.00	27 ± 6	0.60
S_1 population at 60 fs (%)	3 ± 2	3 ± 2	1.00	7 ± 3	0.01	1 ± 1	0.11	11 ± 4	0.00	2 ± 2	0.77
Planar $S_1 \rightarrow S_0$ hop (%)	90 ± 6	92 ± 5	0.82	88 ± 6	0.85	93 ± 5	0.68	84 ± 7	0.32	92 ± 5	0.76
Tw-Stretched $S_1 \rightarrow S_0$ hop (%)	4 ± 4	4 ± 4	1.00	5 ± 4	0.91	5 ± 4	0.90	6 ± 5	0.76	4 ± 4	1.00
Tw-Shrunk $S_1 \rightarrow S_0$ hop (%)	6 ± 5	4 ± 4	0.76	8 ± 5	0.81	2 ± 3	0.23	10 ± 6	0.51	4 ± 4	0.67

4.2 Nonadiabatic dynamics of PSB4

PSB4 is a prototypical example of retinal protonated Schiff base (rPSB), a chromophore of the rhodopsins family which plays a crucial role in the primary step of vision.[58-61] Beyond its biological relevance, PSB4 has been utilized as a model system for studying *cis-trans* photoisomerization due to its ultrafast dynamics.[58, 59] Previous research has investigated in detail the dynamics of PSB4.[45, 62, 63] In the present work, our goal is not to discuss PSB4 photophysics but rather to employ it as a case model to explore the surface hopping dynamics using various velocity adjustments directions.

Like other rPSBs,[60] the first step in PSB4 dynamics following photoexcitation to S_1 (a charge-transfer state) involves unlocking the C=C bond. Subsequent nuclear relaxation leads to an inversion of the single and double bond length alternation along the conjugated chain, typically occurring on a time

scale of 20 fs.[45, 60, 61] It has also been suggested that the proximity with the S_2 state (characterized by a nonreactive diradical character) can influence the unlocking mechanism and significantly affect the dynamics of rPSBs.[61, 64] This mixing between the states can modulate the dynamical evolution along the C–C bonds twisting, leading to photoisomerization. However, exploring this effect is out of the scope of this work. After the skeletal stretching, the nuclear propagation of PSB4 towards photoisomerization on the S_1 surface can follow different pathways involving different conical intersections with the S_0 state.[45]

Figure 3 shows the possible motions leading to the deactivation of *cis*-PSB4. One-bond flip (OBF) is the simplest way to perform *cis-trans* isomerization in a nonrestricted environment.[65, 66] When geometrical restrictions are present (like when the molecule is linked to a protein), alternative mechanisms can take place, involving more than one torsion. The main of them are bicycle-pedal (BP),[67] consisting of simultaneous rotations of two neighbours formal double bonds, nonrigid BP (NRBP),[68-71] which resembles BP, but where one of the torsions proceed only partially, or yet hula-twist (HT),[72] consisting of simultaneous torsions of two adjacent bonds. This last, however, is more often observed in heavily restricted systems.[45, 73] Additionally, the folding table (FT) mechanism, a combination of three torsions with the main one accompanied by two partial rotations, has also been proposed as a volume-conserving process.[74]

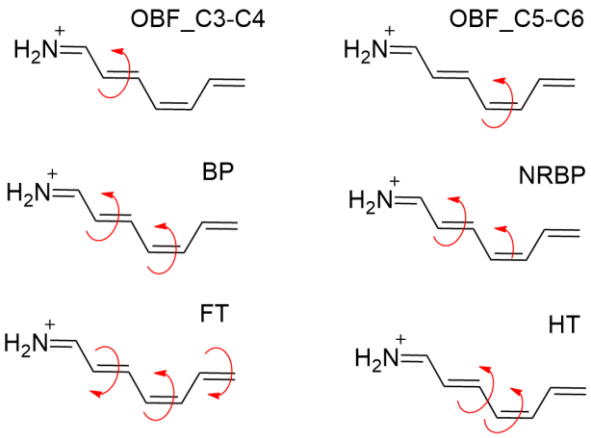

Figure 3. Main torsional motions involved in the photoisomerization of PSB4: OBF, HT, BP, NRBP, and FT.

The decay of the excited state population using different velocity adjustments is depicted in **Figure 4**. All the curves exhibit a similar pattern: initially, a plateau is observed during the first ~50 fs of simulation. It can be associated with the initial skeleton relaxation along the bond length alternation. Subsequently, this relaxation is followed by torsions around one or more bonds. The excited state lifetime is determined using the exponential decay function in Eq. (9). The resulting lifetimes are compiled in **Table 3**. Notably, all the datasets provided lifetimes around 120 fs, in excellent agreement

with previously calculated results (114 fs)[45] and consistent with the lifetime computed for PSB3 at MS-CASPT2 level.[62]

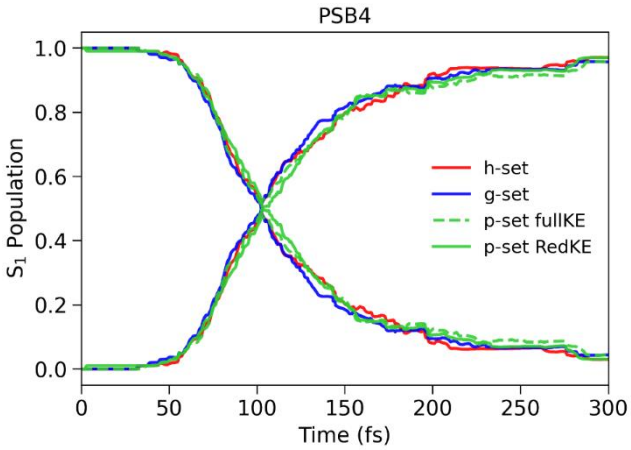

Figure 4. Decay of the excited state population of PSB4 computed with different velocity adjustments after hoppings.

Table 3 also summarizes the ratio of trajectories following the different isomerization channels, classified as described in the Computational Methods. Across all datasets, the NRBP dominates, followed by the OBF (C5–C6) and then the BP and OBF (C4–C3) mechanisms. Together, these mechanisms account for most of the decay pathways for PSB4. The sum of the concerted twist around two double bonds (NRBP and BP) contributes to ~50%, and one bond flip (the sum of OBF (C5–C6) and (C3–C4)) channels contributes to ~40% of the total number of trajectories. This behaviour is expected in nonrestricted systems, as the molecule can freely twist. The FT mechanism is statistically insignificant, and HT was not observed in any of the trajectories. In all datasets, roughly 6% of the trajectories exhibit movements other than those described in **Table S2**, *i.e.*, involving rotational pattern combinations not presented in this table. A small portion of the trajectories ($\leq$ 3%) do not show any hops and are trapped in the excited state within the 300 fs of simulation.

As with fulvene, we compared the datasets using the overlap function (Section 3.3). For PSB4, we considered five observables: the excited state lifetime and the predominant channels for the excited population decay. All four datasets exhibit overlap functions above 0.9 for the computed lifetime, indicating the excellent performance of all velocity adjustment directions for calculating the population decay. The overlap score is also significant for the NRBP channel ($\geq$ 0.88) in all data sets. However, it drops to 0.68 for the OBF(C5–C6) and BP channels in the **p**-adjusted with reduced kinetic energy dataset. In general, **g**-adjustment shows the most robust performance, with λ_x^h greater than 0.85 for all observables. Comparing the two datasets adjusted in the **p**-direction, it becomes evident that the one considering full kinetic energy slightly outperforms the reduced kinetic energy one.

Table 3. Mean value and error bars (95% confidence interval) of time constants, populations, and structural yields computed for PSB4 dynamics with different velocity adjustments after a hopping event. Results for **h**-adjusted, **g**-adjusted, and **p**-adjusted using full kinetic energy (*fullKE*) and reduced kinetic energy (*RedKE*). λ_x^h is the overlap score for each observable computed between **h**-adjusted (at CASSCF level) and the respective dataset.

Observable	h dataset	g dataset	λ_x^h	p *FullKE* dataset	λ_x^h	p *RedKE* dataset	λ_x^h	Ref. [45]
Lifetimes (fs)	120 ± 12	118 ± 12	0.95	123 ± 13	0.91	123 ± 13	0.91	114
OBF (C5-C6) (%)	37 ± 9	34 ± 9	0.86	38 ± 9	0.97	32 ± 9	0.68	25
OBF (C3-C4) (%)	6 ± 5	6 ± 5	1.00	7 ± 5	0.93	6 ± 5	1.00	11
BP hop (%)	7 ± 5	7 ± 5	1.00	7 ± 5	1.00	10 ± 6	0.68	14
NRBP hop (%)	44 ± 10	46 ± 10	0.93	41 ± 10	0.88	41 ± 10	0.88	44

Following the classification of the hopping times, we optimized the conical intersections corresponding to each one of the decay pathways outlined in **Table 3**. The geometry optimization led to four different minima on the crossing seam, whose topographies are shown in **Figure S3** and the parameters summarized in **Table S3.** The first observation is that starting the optimization from hopping geometries that fall in the NRBP classification ends up in the BP conical intersection. This is a peaked conical intersection, while the OBF conical intersections are sloped.

A fundamental question arising after these analyses is: why is fulvene sensitive to the velocity adjustment direction, but PSB4 is not? The answer is connected to the topography of the conical intersections, which, in turn, impacts the number of back hoppings. In fulvene, most of the population decays through a strongly sloped conical intersection; in PSB4, 50% decays via a peaked conical intersection, while 40% decays via a sloped intersection. Furthermore, comparing the slope of planar conical intersections in fulvene with the OBF intersections in PSB4, the former is more sloped. This can be seen in the plot of the conical intersections and the tilt parameters (σ_x and σ_x), which are near zero for PSB4 and have larger values for fulvene. Back hoppings tend to be less likely near a peaked intersection because the energy gap quickly increases after hopping to the lower state. Thus, size extensivity errors—which are caused by back hoppings—tend to be smaller in such systems.

4.3 Evaluation of nonadiabatic coupling vector approximations

4.3.1 Curvature-approximated coupling vector

Recent work from Shu *et al.*[26] proposed a method to compute surface hopping dynamics without computing overlap integrals but only energies of the adiabatic states and their gradients. This method, namely curvature-driven trajectory surface hopping (κTSH), is closely related to the time-dependent Baeck-An (TD-BA) approximation.[21] Besides the fact that TD-BA uses a higher-order approximation to the time second derivatives than κTSH, the main difference between the two approaches is that

κTSH also proposed a way to get an approximated nonadiabatic coupling vector ($\mathbf{G}_{IJ}^{\kappa}$). In this section, we compare $\mathbf{G}_{IJ}^{\kappa}$ with the exact coupling vector provided by our **h**-adjusted dataset to investigate how well this approximation reproduces the vector direction for fulvene. More details are given in the Supporting Information **(Section SI-4)**. For simplification, in our discussion we refer to $\mathbf{G}_{IJ}^{\kappa}$ simply as **G.**

Ref.[26] defines the curvature-driven effective nonadiabatic coupling vector as $\mathbf{G} = \mathbf{g} + \alpha\mathbf{v}$. Here, **g** is the difference gradient vector, **v** is the velocity, and α is a parameter influenced by the time-derivative coupling approximation. In κTSH, the velocity is rescaled in the direction of the difference gradient vector after a successful hop; when a hop is frustrated by the conservation of momentum or energy, the same choices presented in traditional FSSH are available.

We compared the norm of **G** with the norm of the nonadiabatic coupling vector **h** and the angles between these two vectors for the same geometries generated in our fulvene dataset considering three cases: (i) all points generated by the dynamics (120*k* geometries), (ii) points restricted to the geometries with large coupling values (($\|\mathbf{h}\| > 2$; 30*k* geometries), and (iii) the hopping geometries.

Figure 5 (a and b) shows the distribution of the angles between **h** and **G** at the hopping time (including frustrated hops) and at all the geometries with the **h** norm bigger than 2. **G** and **h** are nearly perpendicular, especially considering only the geometries with large couplings. By definition, the angle between the curvature-approximated coupling vector **G** and **g** depends on the parameter α. Therefore, this angle may vary according to the time-derivative coupling. Indeed, we can see in **Figure S5** that the angle changes strongly at the first 20 fs. Still, the oscillation decreases after this time, rendering **G** almost parallel to **g**. We can also see that the angle between **h** and **G**, **g**, or **v** vectors are nearly perpendicular in all cases. These results show that **G** is not a good approximation to the **h** direction. Nevertheless, precisely due to the similarity between these vectors, velocity adjustment in this direction should be as good as using the **g** direction.

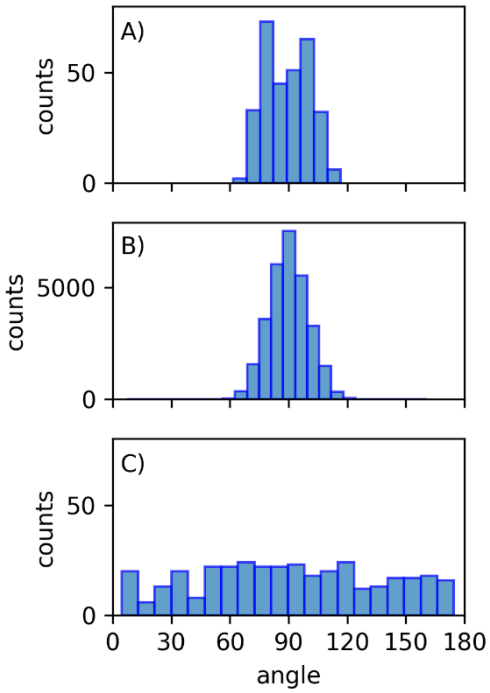

Figure 5. Distribution of the angles between **a)** the exact **h**-vector and the curvature-approximated vector (**G**) at the hopping time (including frustrated hops); **b)** the exact **h**-vector and the curvature-approximated vector (**G**) at all the points with large couplings (||**h**|| > 2); **c)** the exact **h**-vector and the **h**-FOMO-CI vector at the hopping times (including frustrated hops).

4.3.2 Semiempirical coupling vector

We compared the angles our hybrid CASSCF/FOMO-CI approach produces between the exact CASSCF and the semiempirical coupling vectors. As mentioned, this approach consists of computing nonadiabatic coupling vectors with the inexpensive semiempirical FOMO-CI at the hopping times to define the velocity adjustment direction. The FSSH probabilities are still computed with the CASSCF coupling vectors. **Figure 5** (c) shows that the angle between $\mathbf{h}_{CAS}$ and $\mathbf{h}_{FOMO}$ is homogeneously distributed over 0 to 180 degrees. However, the population decay evolution is in close agreement with the **h**-dataset.

Nevertheless, to estimate how similar those two vector's directions are, we may look at the projection, as outlined in Ref. [28], with 0 indicating perpendicular and 1 parallel direction. When we construct a histogram containing the projection of angles between pairs of random vectors going from low (2D) to higher (20D) dimensions (**Figure S10**), we observe an increasing concentration of angles around 90º. Therefore, the fact that $\mathbf{h}_{CAS}$ and $\mathbf{h}_{FOMO}$ are homogeneously distributed in a broad range of angles means that they are pointing somewhat in similar directions rather than in random directions, as we would intuitively expect.

5 Conclusions

This work investigated the impact of post-hopping velocity adjustment directions in surface hopping dynamics. We used fulvene and PSB4 as test cases. Following the decay population of fulvene, a pronounced peak in the region 15-25 fs appears when the velocity is adjusted in the momentum direction **p**, a size-extensivity artefact caused by an artificial excess of back hoppings. Such a peak is much less intense if the velocity is appropriately adjusted in the nonadiabatic coupling vector direction **h**. When we change the velocity in the gradient difference direction **g** or still adjust in the **p** direction but use a reduced kinetic energy reservoir, this peak intensity is attenuated, and the results match the reference well.

PSB4 nonadiabatic dynamics is much less prone to size-extensivity errors caused by the velocity adjustment direction. This difference between the two molecules is that conical intersections in PSB4 are much less sloped than in fulvene. Thus, in PSB4, any artificial excess of back hoppings is naturally inhibited by the fast energy gap growth when it jumps to the ground state. All tested alternative adjustment schemes, **g**-direction or **p**-direction with or without reduced kinetic energy, give satisfactory and similar results.

We also investigated the performance of two inexpensive methods to approximate the nonadiabatic coupling vector direction. The first was the coupling vector predicted by the curvature-driven κTSH method, which is immediately available if **g** is computed. The other was nonadiabatic coupling vectors predicted with the semiempirical FOMO-CI method, which requires an additional low-cost electronic structure calculation.

The comparison of exact nonadiabatic coupling and the curvature-driven effective nonadiabatic coupling shows that they tend to be closer to **g** than **h**. However, they eliminate size-extensivity velocity adjustment errors, as an adjustment in the **g** direction also does. On the other hand, the semiempirical coupling vectors tend to be closer to the exact **h** despite their large statistical variability. They also avoid size extensivity errors.

The statistical analysis showed that **g** is the best alternative direction for velocity adjustment and should be favoured when nonadiabatic coupling vectors **h** are unavailable. Its good performance is likely related to the fact that both **g** and **h** are vectors defining the branching plane around the conical intersection. The curvature-driven vector from κTSH does not perform better than **g**, adding a slight overhead to the calculations. The semiempirical vector also did not work better than **g**. Still, it can be an alternative if **g** cannot be computed. Adjusting the **p** direction with the reduced kinetic energy reservoir is the most cost-effective but with the handicap of being an *ad hoc* approximation. We emphazise that this approximation only impacts the number of back hoppings without interfering with other dynamic features. It is only used to decide whether back hoppings would be allowed.

Finally, our results showed that the adjustment direction is far less important than the size of the kinetic energy reservoir. Every tested method yielded a satisfactory population decay, at least for fulvene, as long they reduced the available kinetic energy for back hoppings. Although we tested this

approach only for fulvene and PSB4 in this work, these two molecules have intrinsically different conical intersection topographies and molecular flexibility. Therefore, we suggest that this procedure should be used in all cases where the velocity adjustment is done in the direction of the momentum.

To summarize, our general recommendation for choosing the velocity adjustment after hoppings in further applications is as follows: the best option is always **h**. When this quantity is unavailable, use the adjustment in the **g**-direction. If this alternative is also unavailable or too expensive, the adjustment should be done in the **p**-direction but using the reduced kinetic energy reservoir. This choice has no implications for the dynamics when there is no excessive number of back hoppings, and it has no extra cost. The same is valid for dynamics using Baeck-An couplings. Our proposed size-extensivity correction prescribes a pragmatic and working solution to decrease the magnitude of a huge kinetic energy reservoir, providing an average kinetic energy per degree of freedom to mimic the velocity adjustment along the unidirectional **h** and **g** vectors.

Data availability

The data that support the findings of this study are openly available online (DOI: 10.5281/zenodo.10024333)

Author Information

Corresponding Authors:

Mario Barbatti – Aix-Marseille University, CNRS, ICR, Marseille, France; Institut Universitaire de France, 75231, Paris, France; Email: mario.barbatti@univ-amu.fr, Website: www.barbatti.org

Josene M. Toldo – Aix-Marseille University, CNRS, ICR, Marseille, France. Email: josene-maria.toldo@univ-amu.fr

Authors:

Rafael de Souza Mattos – Aix-Marseille University, CNRS, ICR, Marseille, France.

Saikat Mukherjee – Aix-Marseille University, CNRS, ICR, Marseille, France.

Max Pinheiro Jr. – Aix-Marseille University, CNRS, ICR, Marseille, France.

Author contributions

Josene M. Toldo: Investigation (lead); Formal analysis (lead); Visualization (lead); Writing – original draft (lead); Writing – review & editing (equal). **Rafael S. Mattos:** (Section 4.3): Investigation, Formal analysis, Visualization, and Writing original draft. **Max Pinheiro:** Investigation (PSB4)**. Saikat Mukherjee**: Software development and Investigation (Section 4.3.2). **Mario Barbatti:**

Conceptualization (lead); Funding acquisition (lead); Methodology (lead); Supervision (lead); Writing – original draft (equal); Writing – review & editing (equal).

Acknowledgements

The authors thank the funding provided by the European Research Council (ERC) Advanced grant SubNano (Grant agreement 832237). J.M.T. and M.B thank funding from the European Union's Horizon 2020 Research and Innovation Program under grant agreement 828753 (Boostcrop). The authors acknowledge Centre de Calcul Intensif d'Aix-Marseille for granting access to its high-performance computing resources. This work was granted access to the HPC resources of TGCC under the allocation 20*22-AD010813035R1* made by GENCI.

Supporting Information

The Supporting Information is available free of charge via the Internet at http://pubs.acs.org.

References

1. Crespo-Otero, R.; Barbatti, M., Recent Advances and Perspectives on Nonadiabatic Mixed Quantum–Classical Dynamics. *Chem. Rev.* **2018,** *118* (15), 7026-7068.
2. Curchod, B. F. E.; Martínez, T. J., Ab Initio Nonadiabatic Quantum Molecular Dynamics. *Chem. Rev.* **2018,** *118* (7), 3305-3336.
3. Tully, J. C., Nonadiabatic molecular dynamics. *Int. J. Quantum Chem.* **1991,** *40* (S25), 299-309.
4. Herman, M. F.; Kluk, E., A Semiclasical Justification for the Use of Non-Spreading Wavepackets in Dynamics Calculations. *Chem. Phys.* **1984,** *91* (1), 27-34.
5. Mukherjee, S.; Barbatti, M., Ultrafast internal conversion without energy crossing. *Results in Chemistry* **2022,** *4*, 100521.
6. Mansour, R.; Mukherjee, S.; Pinheiro, M., Jr.; Noble, J. A.; Jouvet, C.; Barbatti, M., Pre-Dewar structure modulates protonated azaindole photodynamics. *Phys. Chem. Chem. Phys.* **2022,** *24* (20), 12346-12353.
7. Smith, B.; Akimov, A. V., Hot Electron Cooling in Silicon Nanoclusters via Landau–Zener Nonadiabatic Molecular Dynamics: Size Dependence and Role of Surface Termination. *J. Phys. Chem. Lett.* **2020,** *11* (4), 1456-1465.
8. Jasper, A. W.; Stechmann, S. N.; Truhlar, D. G., Fewest-switches with time uncertainty: A modified trajectory surface-hopping algorithm with better accuracy for classically forbidden electronic transitions. *J. Chem. Phys.* **2002,** *116* (13), 5424-5431.
9. Qiu, T.; Climent, C.; Subotnik, J. E., A Practical Approach to Wave Function Propagation, Hopping Probabilities, and Time Steps in Surface Hopping Calculations. *J. Chem. Theory Comput.* **2023,** *19* (10), 2744-2757.
10. Herman, M. F., A Semiclassical Surface Hopping Propagator for Nonadiabatic Problems. *J. Chem. Phys.* **1995,** *103* (18), 8081-8097.
11. Herman, M. F., Nonadiabatic semiclassical scattering. I. Analysis of generalized surface hopping procedures. *J. Chem. Phys.* **1984,** *81* (2), 754-763.
12. Herman, M. F., Optimal representation for semiclassical surface hopping methods. *J. Chem. Phys.* **1999,** *110* (9), 4141-4151.
13. Pechukas, P., Time-Dependent Semiclassical Scattering Theory. II. Atomic Collisions. *Phys. Rev.* **1969,** *181* (1), 174-185.

14. Merritt, I. C. D.; Jacquemin, D.; Vacher, M., Nonadiabatic Coupling in Trajectory Surface Hopping: How Approximations Impact Excited-State Reaction Dynamics. *J. Chem. Theory Comput.* **2023,** *19* (6), 1827-1842.
15. Granucci, G.; Persico, M.; Toniolo, A., Direct Semiclassical Simulation of Photochemical Processes with Semiempirical Wave Functions. *J. Chem. Phys.* **2001,** *114* (24), 10608-10615.
16. Plasser, F.; Granucci, G.; Pittner, J.; Barbatti, M.; Persico, M.; Lischka, H., Surface Hopping Dynamics Using a Locally Diabatic Formalism: Charge Transfer in the Ethylene Dimer Cation and Excited State Dynamics in the 2-Pyridone Dimer. *J. Chem. Phys.* **2012,** *137* (22), 22A514-13.
17. Hammes-Schiffer, S.; Tully, J. C., Proton transfer in solution: Molecular dynamics with quantum transitions. *J. Chem. Phys.* **1994,** *101* (6), 4657-4667.
18. Plasser, F.; Crespo-Otero, R.; Pederzoli, M.; Pittner, J.; Lischka, H.; Barbatti, M., Surface Hopping Dynamics with Correlated Single-Reference Methods: 9H-Adenine as a Case Study. *J. Chem. Theory Comput.* **2014,** *10*, 1395-1405.
19. Belyaev, A. K.; Lebedev, O. V., Nonadiabatic Nuclear Dynamics of Atomic Collisions Based on Branching Classical Trajectories. *Journal of Physics: Conference Series* **2012,** *388* (9), 092007.
20. Suchan, J.; Janos, J.; Slavicek, P., Pragmatic Approach to Photodynamics: Mixed Landau-Zener Surface Hopping with Intersystem Crossing. *J. Chem. Theory Comput.* **2020,** *16* (9), 5809-5820.
21. T. do Casal, M.; Toldo, J. M.; Pinheiro Jr, M.; Barbatti, M., Fewest switches surface hopping with Baeck-An couplings [version 1; peer review: 3 approved]. *Open Research Europe* **2021,** *1*, 49.
22. Yue, L.; Yu, L.; Xu, C.; Lei, Y.; Liu, Y.; Zhu, C., Benchmark Performance of Global Switching versus Local Switching for Trajectory Surface Hopping Molecular Dynamics Simulation: Cis↔Trans Azobenzene Photoisomerization. *ChemPhysChem* **2017,** *18* (10), 1274-1287.
23. Duncan, W. R.; Craig, C. F.; Prezhdo, O. V., Time-Domain ab Initio Study of Charge Relaxation and Recombination in Dye-Sensitized TiO2. *J. Am. Chem. Soc.* **2007,** *129* (27), 8528-8543.
24. Barbatti, M., Velocity Adjustment in Surface Hopping: Ethylene as a Case Study of the Maximum Error Caused by Direction Choice. *J. Chem. Theory Comput.* **2021,** *17* (5), 3010-3018.
25. Braun, G.; Borges Jr, I.; Aquino, A.; Lischka, H.; Plasser, F.; do Monte, S. A.; Ventura, E.; Mukherjee, S.; Barbatti, M., Non-Kasha fluorescence of pyrene emerges from a dynamic equilibrium between excited states. *J. Chem. Phys.* **2022,** *157* (15), 154305.
26. Shu, Y.; Zhang, L.; Chen, X.; Sun, S.; Huang, Y.; Truhlar, D. G., Nonadiabatic Dynamics Algorithms with Only Potential Energies and Gradients: Curvature-Driven Coherent Switching with Decay of Mixing and Curvature-Driven Trajectory Surface Hopping. *J. Chem. Theory Comput.* **2022,** *18* (3), 1320-1328.
27. Ibele, L. M.; Curchod, B. F. E., A molecular perspective on Tully models for nonadiabatic dynamics. *Phys. Chem. Chem. Phys.* **2020**.
28. Barbatti, M., Velocity Adjustment in Surface Hopping: Ethylene as a Case Study of the Maximum Error Caused by Direction Choice. *J. Chem. Theory Comput.* **2021**.
29. Limbu, D. K.; Shakib, F. A., Real-Time Dynamics and Detailed Balance in Ring Polymer Surface Hopping: The Impact of Frustrated Hops. *J. Phys. Chem. Lett.* **2023**, 8658-8666.
30. Alfonso-Hernandez, L.; Athanasopoulos, S.; Tretiak, S.; Miguel, B.; Bastida, A.; Fernandez-Alberti, S., Vibrational energy redistribution during donor–acceptor electronic energy transfer: criteria to identify subsets of active normal modes. *Phys. Chem. Chem. Phys.* **2020,** *22* (33), 18454-18466.
31. Shenai, P. M.; Fernandez-Alberti, S.; Bricker, W. P.; Tretiak, S.; Zhao, Y., Internal Conversion and Vibrational Energy Redistribution in Chlorophyll A. *J. Phys. Chem. B* **2016,** *120* (1), 49-58.
32. Klaffki, N.; Weingart, O.; Garavelli, M.; Spohr, E., Sampling excited state dynamics: influence of HOOP mode excitations in a retinal model. *Phys. Chem. Chem. Phys.* **2012,** *14* (41), 14299-14305.
33. Sellner, B.; Barbatti, M.; Lischka, H., Dynamics starting at a conical intersection: application to the photochemistry of pyrrole. *J. Chem. Phys.* **2009,** *131* (2), 024312.

34. Plasser, F.; Mai, S.; Fumanal, M.; Gindensperger, E.; Daniel, C.; González, L., Strong Influence of Decoherence Corrections and Momentum Rescaling in Surface Hopping Dynamics of Transition Metal Complexes. *J. Chem. Theory Comput.* **2019,** *15* (9), 5031-5045.
35. Ditchfield, R.; Hehre, W. J.; Pople, J. A., Self-Consistent Molecular-Orbital Methods. IX. Extended Gaussian-Type Basis for Molecular-Orbital Studies of Organic Molecules. *J. Chem. Phys.* **1971,** *54* (2), 724-728.
36. Lischka, H.; Shepard, R.; Müller, T.; Szalay, P. G.; Pitzer, R. M.; Aquino, A. J. A.; Araújo do Nascimento, M. M.; Barbatti, M.; Belcher, L. T.; Blaudeau, J.-P.; Borges, I.; Brozell, S. R.; Carter, E. A.; Das, A.; Gidofalvi, G.; González, L.; Hase, W. L.; Kedziora, G.; Kertesz, M.; Kossoski, F.; Machado, F. B. C.; Matsika, S.; do Monte, S. A.; Nachtigallová, D.; Nieman, R.; Oppel, M.; Parish, C. A.; Plasser, F.; Spada, R. F. K.; Stahlberg, E. A.; Ventura, E.; Yarkony, D. R.; Zhang, Z., The generality of the GUGA MRCI approach in COLUMBUS for treating complex quantum chemistry. *J. Chem. Phys.* **2020,** *152* (13), 134110.
37. Lischka, H.; Shepard, R.; Shavitt, I.; Pitzer, R. M.; Dallos, M.; Müller, T.; Szalay, P. G.; Brown, F. B.; Ahlrichs, R.; Böhm, H. J.; Chang, A.; Comeau, D. C.; Gdanitz, R.; Dachsel, H.; Ehrhardt, C.; Ernzerhof, M.; Höchtl, P.; Irle, S.; Kedziora, G.; Kovar, T.; Parasuk, V.; Pepper, M. J. M.; Scharf, P.; Schiffer, H.; Schindler, M.; Schüler, M.; Seth, M.; Stahlberg, E. A.; Zhao, J.-G.; Yabushita, S.; Zhang, Z.; Barbatti, M.; Matsika, S.; Schuurmann, M.; Yarkony, D. R.; Brozell, S. R.; Beck, E. V.; Blaudeau, J.-P.; Ruckenbauer, M.; Sellner, B.; Plasser, F.; Szymczak, J. J.; Spada, R. F. K.; Das, A., COLUMBUS, an ab initio electronic structure program, release 7.0. *Available via the Internet at www.univie.ac.at/columbus*. **2017**.
38. Tully, J. C., Molecular dynamics with electronic transitions. *J. Chem. Phys.* **1990,** *93* (2), 1061-1071.
39. Granucci, G.; Persico, M., Critical appraisal of the fewest switches algorithm for surface hopping. *J. Chem. Phys.* **2007,** *126* (13), 134114.
40. Barbatti, M.; Bondanza, M.; Crespo-Otero, R.; Demoulin, B.; Dral, P. O.; Granucci, G.; Kossoski, F.; Lischka, H.; Mennucci, B.; Mukherjee, S.; Pederzoli, M.; Persico, M.; Pinheiro Jr, M.; Pittner, J.; Plasser, F.; Sangiogo Gil, E.; Stojanovic, L., Newton-X Platform: New Software Developments for Surface Hopping and Nuclear Ensembles. *J. Chem. Theory Comput.* **2022**.
41. Swope, W. C.; Andersen, H. C.; Berens, P. H.; Wilson, K. R., A computer simulation method for the calculation of equilibrium constants for the formation of physical clusters of molecules: Application to small water clusters. *J. Chem. Phys.* **1982,** *76* (1), 637-649.
42. Granucci, G.; Toniolo, A., Molecular gradients for semiempirical CI wavefunctions with floating occupation molecular orbitals. *Chem. Phys. Lett.* **2000,** *325* (1), 79-85.
43. Granucci, G.; Persico, M.; Toniolo, A., Direct semiclassical simulation of photochemical processes with semiempirical wave functions. *J. Chem. Phys.* **2001,** *114* (24), 10608-10615.
44. Stewart, J. *MOPAC2002; Fujitsu Limited: Tokyo, Japan, 2002*.
45. Szymczak, J. J.; Barbatti, M.; Lischka, H., Is the Photoinduced Isomerization in Retinal Protonated Schiff Bases a Single- or Double-Torsional Process? *J. Phys. Chem. A* **2009,** *113* (43), 11907-11918.
46. Granucci, G.; Persico, M., Critical appraisal of the fewest switches algorithm for surface hopping. *J. Chem. Phys.* **2007,** *126* (13), 134114.
47. Bearpark, M. J.; Bernardi, F.; Olivucci, M.; Robb, M. A.; Smith, B. R., Can Fulvene S1 Decay Be Controlled? A CASSCF Study with MMVB Dynamics. *J. Am. Chem. Soc.* **1996,** *118* (22), 5254-5260.
48. Bearpark, M. J.; Blancafort, L.; Paterson, M. J., Mapping the intersection space of the ground and first excited states of fulvene. *Mol. Phys.* **2006,** *104* (5-7), 1033-1038.
49. Blancafort, L., Photochemistry and Photophysics at Extended Seams of Conical Intersection. *ChemPhysChem* **2014,** *15* (15), 3166-3181.

50. Barbatti, M., Velocity Adjustment in Surface Hopping: Ethylene as a Case Study of the Maximum Error Caused by Direction Choice *J. Chem. Theory Comput.* **2021**, DOI:10.1021/acs.jctc.1c00012.
51. Grohmann, T.; Deeb, O.; Leibscher, M., Quantum separation of para- and ortho-fulvene with coherent light: The influence of the conical intersection. *Chem. Phys.* **2007,** *338* (2), 252-258.
52. Belz, S.; Grohmann, T.; Leibscher, M., Quantum dynamical simulations for nuclear spin selective laser control of ortho- and para-fulvene. *J. Chem. Phys.* **2009,** *131* (3), 034305.
53. Alfalah, S.; Belz, S.; Deeb, O.; Leibscher, M.; Manz, J.; Zilberg, S., Photoinduced quantum dynamics of ortho- and para-fulvene: Hindered photoisomerization due to mode selective fast radiationless decay via a conical intersection. *J. Chem. Phys.* **2009,** *130* (12), 124318.
54. Blancafort, L.; Gatti, F.; Meyer, H.-D., Quantum dynamics study of fulvene double bond photoisomerization: The role of intramolecular vibrational energy redistribution and excitation energy. *J. Chem. Phys.* **2011,** *135* (13), 134303.
55. Ruiz-Barragan, S.; Blancafort, L., Photophysics of fulvene under the non-resonant stark effect. Shaping the conical intersection seam. *Faraday Discuss.* **2013,** *163* (0), 497-512.
56. Mendive-Tapia, D.; Lasorne, B.; Worth, G. A.; Bearpark, M. J.; Robb, M. A., Controlling the mechanism of fulvene S1/S0 decay: switching off the stepwise population transfer. *Phys. Chem. Chem. Phys.* **2010,** *12* (48), 15725-15733.
57. Mendive-Tapia, D.; Lasorne, B.; Worth, G. A.; Robb, M. A.; Bearpark, M. J., Towards converging non-adiabatic direct dynamics calculations using frozen-width variational Gaussian product basis functions. *J. Chem. Phys.* **2012,** *137* (22), 22A548.
58. Schoenlein, R.; Peteanu, L.; Mathies, R.; Shank, C., The first step in vision: femtosecond isomerization of rhodopsin. *Science* **1991,** *254* (5030), 412-415.
59. Kukura, P.; McCamant, D. W.; Yoon, S.; Wandschneider, D. B.; Mathies, R. A., Structural observation of the primary isomerization in vision with femtosecond-stimulated Raman. *Science* **2005,** *310* (5750), 1006-1009.
60. Olivucci, M.; Tran, T.; Worth, G. A.; Robb, M. A., Unlocking the Double Bond in Protonated Schiff Bases by Coherent Superposition of S1 and S2. *J. Phys. Chem. Lett.* **2021,** *12* (23), 5639-5643.
61. Gozem, S.; Luk, H. L.; Schapiro, I.; Olivucci, M., Theory and Simulation of the Ultrafast Double-Bond Isomerization of Biological Chromophores. *Chem. Rev.* **2017,** *117* (22), 13502-13565.
62. Zhang, X.; Herbert, J. M., Nonadiabatic dynamics with spin-flip vs linear-response time-dependent density functional theory: A case study for the protonated Schiff base C5H6NH2+. *J. Chem. Phys.* **2021,** *155* (12), 124111.
63. Kandori, H.; Shichida, Y.; Yoshizawa, T., Photoisomerization in Rhodopsin. *Biochemistry (Moscow)* **2001,** *66* (11), 1197-1209.
64. Manathunga, M.; Yang, X.; Orozco-Gonzalez, Y.; Olivucci, M., Impact of Electronic State Mixing on the Photoisomerization Time Scale of the Retinal Chromophore. *J. Phys. Chem. Lett.* **2017,** *8* (20), 5222-5227.
65. González-Luque, R.; Garavelli, M.; Bernardi, F.; Merchán, M.; Robb, M. A.; Olivucci, M., Computational evidence in favor of a two-state, two-mode model of the retinal chromophore photoisomerization. *Proceedings of the National Academy of Sciences* **2000,** *97* (17), 9379-9384.
66. Vreven, T.; Bernardi, F.; Garavelli, M.; Olivucci, M.; Robb, M. A.; Schlegel, H. B., Ab Initio Photoisomerization Dynamics of a Simple Retinal Chromophore Model. *J. Am. Chem. Soc.* **1997,** *119* (51), 12687-12688.
67. Warshel, A., Bicycle-pedal model for the first step in the vision process. *Nature* **1976,** *260* (5553), 679-683.
68. Schapiro, I.; Weingart, O.; Buss, V., Bicycle-pedal isomerization in a rhodopsin chromophore model. *J. Am. Chem. Soc.* **2009,** *131* (1), 16-17.
69. Hayashi, S.; Tajkhorshid, E.; Schulten, K., Photochemical reaction dynamics of the primary event of vision studied by means of a hybrid molecular simulation. *Biophys. J.* **2009,** *96* (2), 403-416.

70. Frutos, L. M.; Andruniów, T.; Santoro, F.; Ferré, N.; Olivucci, M., Tracking the excited-state time evolution of the visual pigment with multiconfigurational quantum chemistry. *Proceedings of the National Academy of Sciences* **2007,** *104* (19), 7764-7769.
71. Andruniów, T.; Ferré, N.; Olivucci, M., Structure, initial excited-state relaxation, and energy storage of rhodopsin resolved at the multiconfigurational perturbation theory level. *Proceedings of the National Academy of Sciences* **2004,** *101* (52), 17908-17913.
72. Liu, R. S.; Asato, A. E., The primary process of vision and the structure of bathorhodopsin: a mechanism for photoisomerization of polyenes. *Proceedings of the National Academy of Sciences* **1985,** *82* (2), 259-263.
73. Sumita, M.; Saito, K., Theoretical study on hula-twist motion of penta-2, 4-dieniminium on the S1 surface under isolated condition by the complete active space self-consistent field theory. *Chem. Phys. Lett.* **2006,** *424* (4-6), 374-378.
74. Szymczak, J. J.; Barbatti, M.; Lischka, H., Mechanism of Ultrafast Photodecay in Restricted Motions in Protonated Schiff Bases: The Pentadieniminium Cation. *J. Chem. Theory Comput.* **2008,** *4* (8), 1189-1199.